ISSN 1063-7834, Physics of the Solid State, 2021, Vol. 63, No. 2, pp. 253–260. © Pleiades Publishing, Ltd., 2021.
Russian Text © The Author(s), 2021, published in Fizika Tverdogo Tela, 2021, Vol. 63, No. 2, pp. 229–236.

MAGNETISM

Features of the Cation Distribution and Magnetic Properties of $BaFe_{12-x}Y_xO_{19}$ Hexaferrites

V. G. Kostishin[a], V. V. Korovushkin[a], I. M. Isaev[a], A. Yu. Mironovich[a], S. V. Trukhanov[b], V. A. Turchenko[c, d, e], K. A. Astapovich[b], and A. V. Trukhanov[a, b, *]

[a] *National Research Technological University (MISiS), Moscow, Russia*
[b] *Scientific-Practical Materials Research Center, National Academy of Sciences of Belarus, Minsk, Belarus*
[c] *Frank Laboratory of Neutron Physics, Joint Institute for Nuclear Research, Dubna, Russia*
[d] *South-Ural State University, Chelyabinsk, Russia*
[e] *Galkin Physics and Technical Institute, National Academy of Sciences of Ukraine, Kiev, Ukraine*
**e-mail: truhanov86@mail.ru*

Received September 6, 2020; revised September 6, 2020; accepted September 9, 2020

Abstract—Using Mössbauer spectroscopy, magnetometry and X-ray diffraction, we have studied the $BaY_xFe_{12-x}O_{19}$ hexaferrite ($0.1 \le x \le 1.2$). The low isomorphic capacitance of hexaferrite is shown, which leads to phase separation with the formation of $BaFe_2O_4$ and $Y_3Fe_5O_{12}$ for $x = 0.6$. Mössbauer spectroscopy data have shown that, in the studied range of substitutions, Y^{3+} ions enter the 12*k* position with the formation of a nonequivalent 12*k*' position due to the breaking of two Fe(12*k*)–O–Fe(12*k*) magnetic bonds in the 12*k* octahedron triad with their replacement by Fe(12*k*)–O–Y (12*k*). The $BaY_xFe_{12-x}O_{19}$ hexaferrite has been shown to be less magnetically hard than $BaFe_{12-x}Al_xO_{19}$.

Keywords: barium hexaferrite, yttrium, Mössbauer spectroscopy, magnetometry, X-ray diffraction, specific magnetization, coercive force, substitution coefficient, nonequivalent positions, structural positions

DOI: 10.1134/S106378342102013X

1. INTRODUCTION

Type-*M* hexagonal ferrites, in particular $BaFe_{12}O_{19}$, are increasingly used in various areas of the electrical and electronic industries. They are used as permanent small-sized magnets in magnetoelectronic and microsystem technology devices, microwave devices, as memory elements, radio-absorbing materials, etc. This is due to their wide isomorphic capacity and a variety of isomorphic elements, which make it possible to vary the magnetic, electrical, mechanical, chemical and other properties of ferrites in a wide range. A crystalline structure of the *M*-type hexaferrites is isomorphic to the natural mineral magnetoplumbite $PbFe_{12}O_{19}$. In hexaferrite structure, iron ions occupy five crystallographic positions: 2*a*, 2*b*, $4f_1$, $4f_2$, and 12*k*. Positions 2*a*, $4f_2$, and 12*k* are octahedral, $4f_1$ is tetrahedral, and 2*b* forms a bipyramid. Polyhedra $4f_1$ and 2*a* are located in the spinel block (*S*), $4f_2$ and 2*b*—in the hexagonal block (*R*), and 12*k* at the boundary of the spinel and hexagonal blocks (*RS*) [1]. An unsubstituted $BaFe_{12}O_{19}$ hexaferrite has a collinear magnetic structure, in which the magnetic moments in positions 12*k*, 2*a*, and 2*b* are directed in one direction, and $4f_1$ and $4f_2$ in the other, antiparallel [2], which leads to an uncompensated antiferromagnetism (ferrimagnetism). Weakening of these interactions due to the substitution of Fe^{3+} ions of both groups by nonmagnetic and/or weakly magnetic ions of metals, leads to a decrease in the resulting magnetic moment. There is a large number of literature data on isovalent single-element isomorphic substitutions in hexaferrites, upon which the electroneutrality charge balance is maintained [3–7].

When treating the incorporation of ittrium in the hexaferrite lattice, many authors, for a more expressed changing of magnetic and electrical properties, explore, along with yttrium, other elements, paired incorporations, such as trivalent and bivalent. For example, in [8], when studying $Sr_{1-x}Mn_xFe_{12-x}Y_xO_{19}$ hexaferrite, using Mössbauer spectroscopy, the authors note an increase in the isomer shift of ions in $4f_1$ and 2*a* positions with increasing *x* from 0.1 to 0.5. In this case, the quadrupole splitting of ions in the $4f_2$ position at $x = 0.3$ changes the sign, the areas of 12*k* and 2*a* sextets decrease, while the area of $4f_2$ increases. An additional sextet appears in the spectrum, the area of which increases with increasing substitution degree *x*. The authors believe that the Mn^{2+} ions not only replace the Ba^{2+} ions, but occupy the 12*k* position at

$x \geq 0.3$ and can likely cause the change in the sign of the Fe^{3+} quadrupole splitting in the $4f_2$ position adjacent to $12k$. However, it is not entirely clear how the charge balance is implemented in this case.

In [9], using the method of complex impedance spectroscopy, the authors investigated the mechanism of ac conductivity and dielectric properties of the $BaBi_xLa_xY_xFe_{12-3x}O_{19}$ hexaferrites ($0 \leq x \leq 0.33$) in the frequency range from 1 Hz to 1 MHz in the temperature range of 20–120°C. The aim of the work was to study the influence of electrical properties of hexaferrites on microwave absorption processes, however, the effect of magnetic properties was not explored in this case.

Magnetic properties of hexaferrite of the same composition were studied in [10]. In this work, a high specific (53.7–67.4 A m^2/kg) and remanent magnetization was found. With increasing the substitution degree, the coercive force in hexaferrite decreases to 2.18 A/m, which allows one to consider hexaferrite to be a sufficiently magnetically hard material.

To study the magnetic properties of $SrBi_xLa_xY_xFe_{12-3x}O_{19}$ hexaferrite ($0 \leq x \leq 0.33$), the authors of [11] used X-ray diffraction, magnetometry, and Mössbauer spectroscopy. In that work, the single-phase composition of hexaferrite, the ferrimagnetic nature of nanoparticles, and a decrease in the coercive force with increasing the content of doping ions were established. Using the data of Mössbauer spectroscopy, the changes in the linewidths, isomeric shift, quadrupole splitting, relative area and magnetic field on Fe^{57} nuclei were determined upon substitutions of Bi^{3+}, La^{3+}, and Y^{3+}.

The direct incorporation of Y^{3+} ions into the hexaferrite structure was investigated in [12, 13]. Using X-ray diffraction and magnetic measurements in the study of $BaY_xFe_{12-x}O_{19}$ hexaferrite ($0 \leq x \leq 1.0$), the authors of [12] noted an increase in the parameters a, b, and c of a unit cell with increasing x from 0 to 0.6 due to the larger radius of Y^{3+} compared to Fe^{3+}, but all parameters decrease at $x > 0.6$. The saturation magnetization increases up to $x = 0.4$, and then decreases, which the authors explain by substitutions in the $4f_1$ and $4f_2$ positions. However, it is difficult to imagine that a large ion Y^{3+} enters the tetrahedron. In this case, the coercive force sharply grows when x varies from 0 to 0.4, and then increases slower. The results obtained are certainly of interest, but many points do not find a convincing explanation, for example, an increase in the coercive force along with magnetization in the range of x less than 0.4 and a decrease in the unit cell parameters at $x > 0.6$. The authors of [13] explored the $Ba_{(1-x)}Y_xFe_{12}O_{19}$ hexaferrite with lower yttrium concentrations ($x = 0$, 0.02, 0.05, 0.08, 0.1, 0.13). Moreover, the authors note an increase in the ratio of the hexaferrite unit cell parameters (c/a), relating these changes with different ionic radii of the Y^{3+} and Fe^{3+} ions, but they assumed that the Ba^{2+} ions are replaced by the Y^{3+} ions. The magnetization first increases in the range of x from 0 to 0.04 and then decreases. The coercive force first increases drastically from 2.1 to 3.5 kOe at $x = 0.04$, and then monotonically increases to 3.7 kOe at $x = 0.13$. In this case, in all samples, starting with $x = 0.05$, an impurity of hematite is detected by X-ray diffraction.

A brief review on M-type hexaferrites doped only with yttrium shows that, on the one hand, there are too few such works, while on the other hand, the analysis of the cationic distribution of iron and yttrium ions in the M-type structure is not complete and there are different interpretations of the results.

The aim of this work is to study the cation distribution in $BaFe_{12-x}Y_xO_{19}$ hexaferrites, compare the isomorphism limits of yttrium with other elements, and assessing its effect on magnetic properties using Mössbauer spectroscopy magnetometry and radiography.

2. OBJECTS AND METHODS OF STUDY

The objects of study were samples of polycrystalline barium hexaferrites $BaFe_{12-x}Y_xO_{19}$, where $x =$ 0.1, 0.3, 0.6, 0.9, 1.2. Samples were fabricated using ceramic technology from ultrapure Fe_2O_3, Y_2O_3 oxides and $BaCO_3$ carbonate. The preliminary initial composition was subjected to synthesizing firing in air at 1200°C (6 h), and then sintering at 1300°C (6 h). After sintering, the samples were cooled slowly in a furnace (~100°C/h) [14]. The Mössbauer spectra of the $BaFe_{12-x}Y_xO_{19}$ samples were recorded in 512 points with constant acceleration using a Ms-1104 Em spectrometer, a Co^{57} γ-spectrometer in chromium matrix at room temperature. Isomeric (chemical) shift was calculated relative to α-Fe. Powder samples from sintered ferrites with a size of 0.05–0.07 mm were used. The mathematical processing of spectra was carried out using the Univem Ms program. Magnetic parameters, such as specific magnetization σ_s, remanent magnetization σ_r, coercive force H_c, and a hysteresis loop shape were measured using a VSM-250 vibration magnetometer in a magnetic field of 20 kOe at 300 K. The phase composition of the samples was determined using a Rigaku Ultima 4 diffractometer with Bragg-Brentano focusing of CuK_α radiation using a graphite monochromator on a diffracted beam. We used the scanning mode by points with angles 2θ in the range of 20°–140° with a step of 0.05°.

3. RESULTS AND DISCUSSION

Figure 1 shows the Mössbauer spectra of the $BaFe_{12-x}Y_xO_{19}$ hexaferrite samples. All spectra were decomposed into constituent sextets using the Univem Ms program. The decomposition model was based on the following. In the substituted ferrites, sextets were allocated belonging to iron ions in the main five posi-

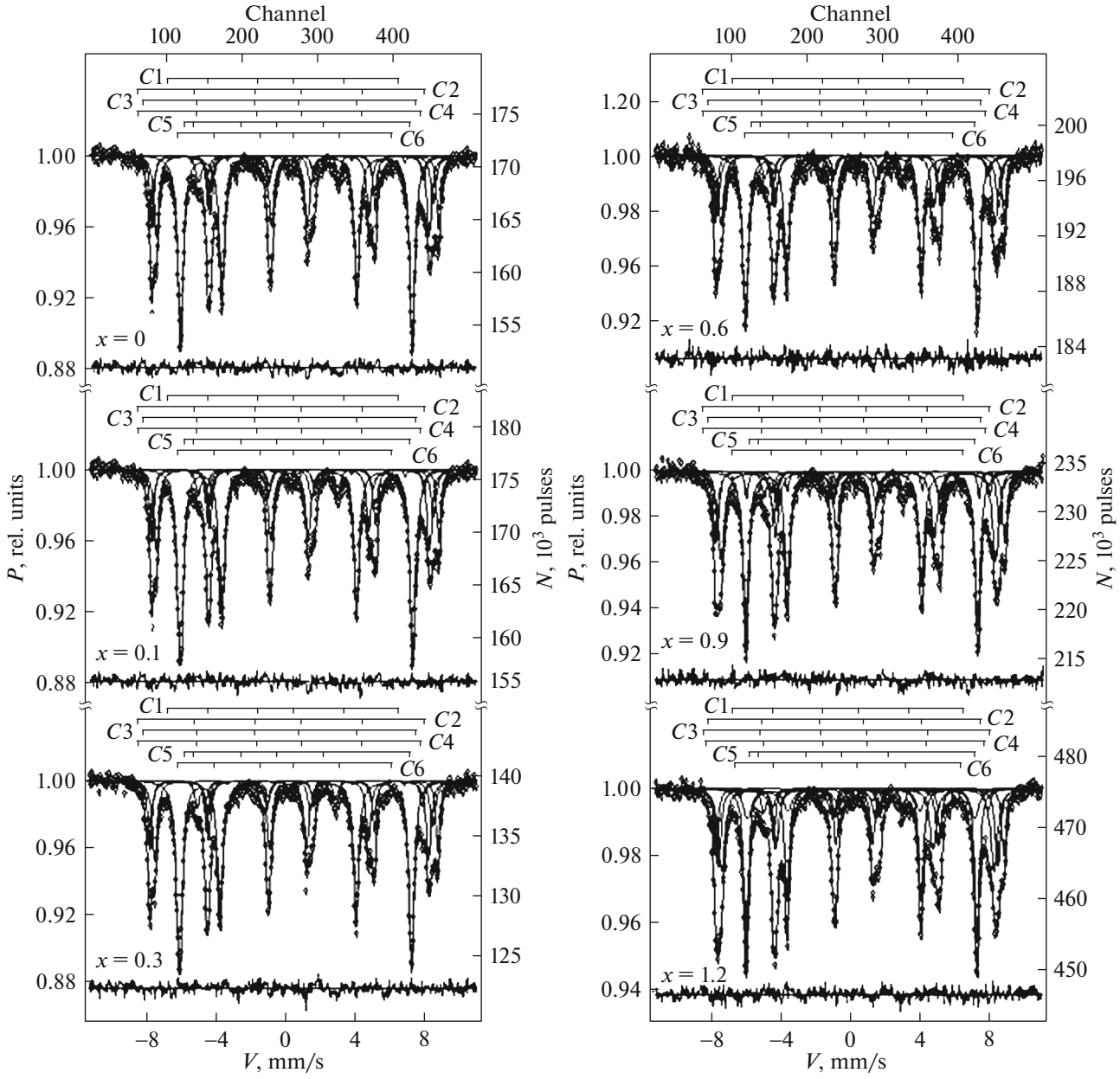

Fig. 1. Mössbauer's spectra of hexagonal ferrites $BaFe_{12-x}Y_xO_{19}$ ($x = 0$, 0.1, 0.3, 0.6, 0.9, 1.2).

tions with parameters of unsubstituted hexaferrite, and the positions of additional sextets were visually determined. The best processing option, according to the program, was determined by parameter $\min\chi^2$ while maintaining the physical meaning of Mössbauer's parameters. The positions occupied by yttrium ions in the structure, and the dangling magnetic bonds of the indirect Fe–O–Fe magnetic exchange were determined from a decrease in the integral sextet peak intensities. In this case, it was taken into account that when a substituting ion occupies the established position in the case of nonequivalent positions of Fe ions, magnetic bonds with neighboring polyhedra can form. It was assumed that an yttrium ion incorporation into the 12*k* position can form two nonequivalent 12*k*' positions by combining three 12*k* octahedra. According to the above considerations, the Mössbauer spectra of all samples were decomposed into six sextets, which means the appearance of one non-equivalent position of the Fe^{3+} ion. This decomposition provided the best values for Pearson's χ^2 criterion. In this case, an increase of the substitution degree *x* was accompanied by an increase in the integral intensity of the additional sextet. The obtained parameters of sextets, namely isomeric (chemical) shift δ (mm/s), quadrupole splitting Δ (mm/s), magnetic field on Fe^{57} nuclei

Table 1. Mössbauer's spectra parameters of $BaFe_{12-x}Y_xO_{19}$

Sample $BaFe_{12-x}Y_xO_{19}$	Spectrum component	Isomeric shift δ, mm/s	Quadrupole splitting Δ, mm/s	Magnetic fields H_{eff}, kOe	Component areas S, %	Bandwidth Γ, mm/s
$x = 0$	$C1(12k)$	0.35	0.42	414	50.5	0.32
	$C2(4f_1)$	0.26	0.22	489	19.8	0.31
	$C3(4f_2)$	0.38	0.20	516	16.8	0.29
	$C4(2a)$	0.34	0.01	507	7.5	0.26
	$C5(2b)$	0.28	2.21	400	5.3	0.30
$x = 0.1$	$C1(12k)$	0.36	0.42	413	48.1	0.37
	$C2(4f_2)$	0.39	0.20	514	13.4	0.27
	$C3(4f_1)$	0.29	0.20	489	19.6	0.35
	$C4(2a)$	0.35	0.00	506	12.3	0.37
	$C5(2b)$	0.30	2.23	401	5.05	0.3
	$C6(12k')$	0.43	0.02	379	1.1	0.21
$x = 0.3$	$C1(12k)$	0.36	0.42	413	47.3	0.37
	$C2(4f_2)$	0.39	0.20	515	13.5	0.27
	$C3(4f_1)$	0.27	0.20	489	19.7	0.35
	$C4(2a)$	0.33	0.01	506	12.9	0.41
	$C5(2b)$	0.29	2.21	401	5.7	0.31
	$C6(12k')$	0.44	0.45	380	0.8	0.23
$x = 0.6$	$C1(12k)$	0.36	0.42	414	42.0	0.35
	$C2(4f_2)$	0.38	0.19	516	11.9	0.24
	$C3(4f_1)$	0.27	0.21	489	21.0	0.41
	$C4(2a)$	0.35	0.04	503	16.0	0.42
	$C5(2b)$	0.30	2.15	398	7.0	0.45
	$C6(12k')$	0.43	0.27	383	2.1	0.23
$x = 0.9$	$C1(12k)$	0.35	0.41	413	41.6	0.36
	$C2(4f_2)$	0.39	0.17	516	13.7	0.30
	$C3(4f_1)$	0.26	0.22	488	22.9	0.42
	$C4(2a)$	0.36	0.01	501	14.8	0.31
	$C5(2b)$	0.32	2.23	400	4.9	0.29
	$C6(12k')$	0.36	0.35	382	2.1	0.23
$x = 1.2$	$C1(12k)$	0.35	0.42	412	34.5	0.36
	$C2(4f_2)$	0.39	0.17	514	11.9	0.28
	$C3(4f_1)$	0.25	0.21	485	23.1	0.46
	$C4(2a)$	0.35	0.04	499	18.5	0.36
	$C5(2b)$	0.29	2.16	400	4.9	0.34
	$C6(12k')$	0.35	0.40	405	7.1	0.38

(H_{eff}, kOe), areas of spectral components S (rel %), resonance line width Γ (mm/s) and their correspondence to the occupied positions are given in Table 1. For comparison, the table shows the parameters of one of the unsubstituted barium hexaferrites.

When analyzing Mössbauer's parameters (Table 1) for both unsubstituted and substituted hexaferrites, one can note the isomeric shift stability, δ (0.35–0.36 mm/s), from Fe^{3+} ions in the $12k$ position and quadrupole splitting (0.41–0.42 mm/s) for sextets 1. For Fe^{3+} ions in octahedral position $4f_2$, the average value δ was 0.39 mm/s, and for Fe^{3+} in the $12k$ and $2a$ positions—0.35 mm/s. Since the value of the isomeric shift increases with an increase in the bond ionicity,

the Fe^{3+} ions in $4f_2$ position are characterized by a higher value than the Fe^{3+} ions in the 12*k* and 2*a* positions.

The Fe^{3+} ions in tetrahedral position $4f_1$ (0.25–0.29 mm/ s) and bipyramidal position 2*b* (0.29 mm/s) demonstrate, in accordance with [15], significantly lower values of δ, which is explained by the greater bond covalence between iron ions due to a smaller volume of the $4f_1$ and 2*b* polyhedra. The quadrupole splitting Δ of Fe^{3+} ions depends only on the electric field gradient of ligands and increases when the symmetry of polyhedra differs from ideal [16]. Therefore, the quadrupole splitting of the Fe^{57} nucleus levels (2.15–2.27 mm/s) is explained by a significant symmetry distortion of the 2*b* polyhedron, while for the most symmetric octahedron 2*a*, the quantity Δ varies in the range (0–0.04 mm/s). The magnetic fields at the Fe^{57} nuclei of all basic positions change insignificantly. With increasing *x*, a slight decrease in the magnetic field is observed on the Fe^{57} nuclei in the 2*a* position, and a jump to 410 kOe in the 12*k*' position at $x = 1.2$. This indicates that the substitutions in hexaferrite are limited. This can be judged by visual assessing the form of the spectra, which does not show significant changes. Changes in the spectra of samples can only be seen when comparing the areas of sextets. As one can see from Table 1, the integral intensity from Fe^{3+} ions in positions 12*k*, 2*a*, $4f_1$ and from additional sextet 12*k*' undergoes a significant change. A slight decrease in the areas of sextets corresponding to Fe^{3+} ions of the bipyramid compared with theoretical values in all samples is explained by the difference in vibration amplitudes of the Fe^{3+} ions in this polyhedron, but not by substitutions. Comparison of the areas of sextets for all five basic positions shows that the area of the sextet corresponding to the ions in the 12*k* position underwent the greatest change. This gave ground to assume that yttrium ions mainly occupy this position, and an additional sextet, designated as 12*k*', is formed due to the breaking of two magnetic bonds Fe(12*k*)–O–Fe (12*k*) in the triad of octahedra 12*k* with their replacement by Fe(12*k*)–O–Y(12*k*). The dynamics of the change in the integral intensities of the sextets corresponding to Fe^{3+} ions can be traced in Fig. 2.

One can allocate two ranges in the integral intensities of the Mössbauer spectra sextets. The first includes the *x* values in the range 0.1–0.9, and the second – in the range 0.9–1.2. In the first interval, significant changes involve a decrease in the intensity of the 12*k* sextets and a slight increase in the intensity of the $4f_1$, 2*a*, and 12*k*' sextets. More significant changes in the sextet intensities can be observed in the second interval: a sharper decrease in the intensity of the 12*k* sextet, a slight decrease in $4f_2$, and an increase in 12*k*', $4f_1$, and 2*a*. In our opinion, this can be explained as follows. Substitutions at the 12*k* position caused the appearance of the 12*k*' sextet, leading to the break of

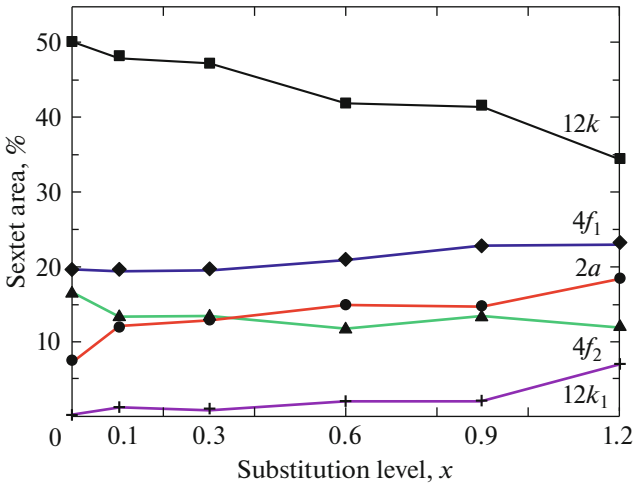

Fig. 2. Dependence of the integral intensities of Mössbauer spectra sextets of $BaFe_{12-x}Y_xO_{19}$ on the substitution degree *x*.

the Fe(12*k*)–O–Fe($4f_2$) magnetic bond. This resulted in a decrease in the intensity of the sextet corresponding to Fe^{3+} ions in the $4f_2$ position. A slight decrease in the magnetic field at the Fe^{57} nuclei in the 2*a* position indicates that Fe(12*k*)–O–Fe(2*a*) bonds are partially broken, and the presence of impurity phases explains the increasing intensities of $4f_1$ and 2*a*. Comparison of the intensities of *M*-type hexaferrite and garnet ferrite showed that the positions of peaks 1 and 6 from octahedral Fe^{3+} ions of the garnet ferrite are very close to the positions of the peaks corresponding to Fe^{3+} ions in position $4f_1$ of hexaferrite. It is this leads to an increase in the area of $4f_1$, in contrast to the data of [13], where the authors believe that yttrium occupies a tetrahedral position. However, in our experiments, we did not observe a decrease in the population of $4f_1$ position for any hexaferrite composition. In addition, we believe that the Y^{3+} ion with a large radius (1.06 Å) cannot enter a tetrahedron with a smaller volume than an octahedron. Similarly, the superposition of peaks from $BaFe_2O_4$ spinel ferrite is possible on the area 2*a*, which increases it in the samples with $x = 0.3–1.2$. The effect of iron-containing impurities on the integral intensities of some sextets was confirmed by X-ray measurements.

The obtained X-ray diffraction patterns of the $BaFe_{12-x}Y_xO_{19}$ samples are shown in Fig. 3, and in Table 2—the registered impurity phases and their quantitative abundances. A small Fe_2O_3 oxide phase (3.3–4.5%) is present in samples of all compositions and does not significantly change Mössbauer's spectra. In this case, yttrium completely enters the hexaferrite lattice, but the $BaFe_2O_4$ phase appears at $x = 0.6$. Its content changes slightly as the degree of substitution increases, but it may contain an impurity of

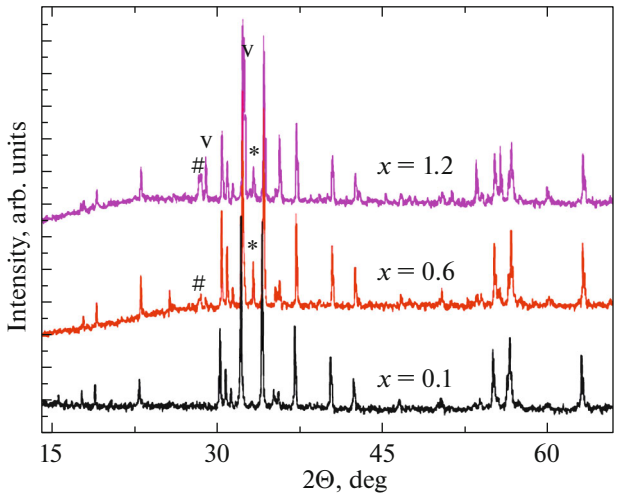

Fig. 3. General view of the X-ray diffraction spectra of $BaFe_{12-x}Y_xO_{19}$ samples ($x = 0.1$, 0.6, and 1.2) obtained at room temperature. The most intense lines are marked, relating to impurity phases: Fe_2O_3 (*), $BaFe_2O_4$ (#), $Y_3Fe_5O_{12}$ (v).

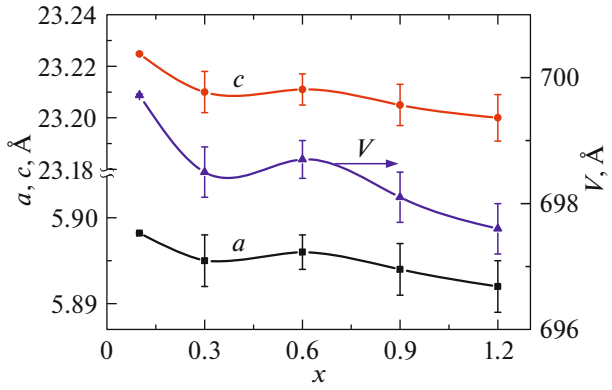

Fig. 4. Concentration dependences of the unit cell parameters of $BaFe_{12-x}Y_xO_{19}$ ($x = 0.1$–1.2).

yttrium. More significant changes in the sample composition appear at $x = 0.9$, when X-ray diffraction determines the appearance of $Y_3Fe_5O_{12}$ garnet-ferrite phase (14.3%), showing that not all of the yttrium occupied the hexaferrite lattice, and the limit of its isomorphic occurrence was reached. At $x = 1.2$, the content of garnet ferrite increases even more and reaches 22%. According to the results obtained, it can be concluded that isomorphic substitutions in $BaFe_{12-x}Y_xO_{19}$ hexaferrite are limited and its isomorphic capacity is significantly lower than upon substitutions with Al, In, Ga, Ti, Zn and other elements. The reason for this is apparently the large ionic radius of the Y^{3+} ion (1.06 Å), in contrast to the elements listed above, as well as the difference in their electronic configuration. The presence of an impurity phase of yttrium garnet-ferrite confirms an increase in the integral intensity of the $4f_1$ sextet, the intensity of which also increases with an increase in x. It should be noted that, judging by the Mössbauer spectra, an increase in the integral intensity of the $4f_1$ sextet starts already at $x = 0.6$, and the entry limit for Y^{3+} ions is possibly lower than $x = 0.9$. A weak reflection from the $Y_3Fe_5O_{12}$ phase one can also see in the X-ray diffraction pattern at $x = 0.6$ and $2\Theta \sim 28°$.

It is of interest to analyze the change in the unit cell parameters of the $BaFe_{12-x}Y_xO_{19}$ hexaferrite shown in Fig. 4. One can see a shurp increase in the unit cell parameters (a, c, v) in the given concentration dependences at $x = 0.6$. This increase is apparently associated with deformation processes in the structure in connection with the onset of the solid solution decomposition. A further increase in the substitution degree x leads to a decrease in all parameters. The drastic increase in the parameters at $x = 0.6$ confirms the above assumption that the limit of isomorphic entry of Y^{3+} ions is $x = 0.6$.

Using magnetic measurements, the dependences of the specific and residual magnetizations, as well as the coercive force as functions of substitution degree x were obtained. The dependences of the specific and residual magnetizations on x are shown in Fig. 5a. They are monotonic in the range of x from 0.1 to 1.2. When estimating the change in the specific magnetization, one can note that it varies insignificantly in this range, by only 9 emu/g, which is significantly less than for other substituting elements. Thus, when Fe^{3+} ions were replaced by Al^{3+} [17] and In^{3+} [5] ions in the same range, the value of σ_s decreased by 18 emu/g, and by

Table 2. Quantitative phase composition of the solid solution samples $BaFe_{12-x}Y_xO_{19}$ ($x = 0.1$–1.2) depending on the concentration of Y ions

Conc. Y^{3+}, x	Phase $BaFe_{12-x}Y_xO_{19}$, %	Phase Fe_2O_3, %	Phase $BaFe_2O_4$, %	Phase $Y_3Fe_5O_{12}$, %
0.1	96.7	3.3	0	0
0.3	95.7	4.3	0	0
0.6	88.6	4.5	6.9	0
0.9	75.5	3.9	6.3	14.3
1.2	68.1	3.3	6.5	22.1

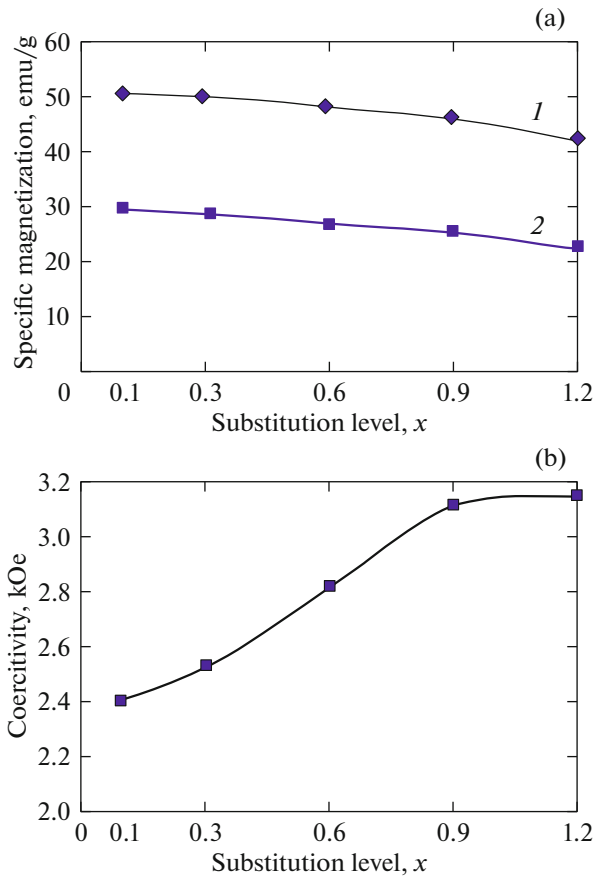

Fig. 5. Magnetic characteristics of $BaFe_{12-x}Y_xO_{19}$: (a) specific magnetization σ_s (*1*) and remanent magnetization σ_r (*2*); (b) coercive force.

27 emu/g when replacing with Ga^{3+} ions [17]. In this case, when Fe^{3+} is replaced by the same elements, the coercive force behaves somewhat differently than in the case of yttrium (Fig. 5b): upon the incorporation of Y^{3+} ions, an increase in H_c from 2.4 to 3.14 kOe is observed, and then the curve becomes flatter in the range $x = 0.9–1.2$. This is consistent with increasing the impurity phases and decreasing isomorphic yttrium in the hexaferrite lattice. If we compare the coercive force change when the Y^{3+} ions are incorporated into the lattice with the cases of Al^{3+} and Ga^{3+}, then one can note the following. Upon substitution with Al^{3+} ions, the coercive force increases from 3.8 to 6.9 kOe, after which it decreases to 4.6 kOe, and upon substitution with Ga^{3+} ions, the H_c decreases from 2 to 0.5 kOe. According to our analysis of the behavior of H_c, $BaFe_{12-x}Al_xO_{19}$ hexaferrite can be classified as a magnetically hard, and $BaFe_{12-x}Ga_xO_{19}$—as soft magnetic ferrite [17]. With this behavior of the coercive force, $BaFe_{12-x}Y_xO_{19}$ hexaferrite occupies an intermediate position, closer to magnetically hard materials. The angle Θ between the magnetic moment of the samples and the direction of the γ-radiation vector is stable and is 56.1°, which indicates the isotropic character of the $BaFe_{12-x}Y_xO_{19}$ samples.

When comparing the effect of Y^{3+}, Al^{3+}, and Ga^{3+} ions on the properties of hexaferrite, one should take into account that the ionic radii of Al^{3+} and Ga^{3+} ions are much smaller than the radius of the Y^{3+} ion. Therefore, first of all, to compare magnetic properties, it is interesting to compare the effect of isomorphic impurities with the same ionic radii. Such ion, comparable in size to Y^{3+}, is In^{3+}. For comparison, we used some results of [5], where the properties of $BaFe_{12-x}In_xO_{19}$ hexaferrite were studied with the same impurity contents and the same research methods were applied.

As follows from a comparison of the results of investigation of $BaFe_{12-x}Y_xO_{19}$ and $BaFe_{12-x}In_xO_{19}$ hexaferrites, despite the identical radii of Y^{3+} and In^{3+} ions, the magnetic properties and structural features of the hexaferrites differ significantly. The isomorphic capacity of $BaFe_{12-x}In_xO_{19}$ hexaferrite is significantly higher than that of $BaFe_{12-x}Y_xO_{19}$. The cation distributions also differ. If the Y^{3+} ions are mainly localized at the positions 12*k*, then the In^{3+} ions are characterized by a disordered distribution in the 2*b*, $4f_2$, and 12*k* sublattices, which leads to a weakening of intersublattice interactions and a noncollinear magnetic structure. In this case, it should be taken into account that the Y^{3+} and In^{3+} ions have electronic configurations $3d^{10}4p^6$ and $4d^85s^2$, and this is also the reason for the differences in the magnetic properties of hexaferrites. Therefore, one can assert that the main reason for different properties of $BaFe_{12-x}Y_xO_{19}$ and $BaFe_{12-x}In_xO_{19}$ hexaferrites are different cation distribution and different electronic configuration of the Y^{3+} and In^{3+} ions.

Thus, investigations of $BaFe_{12-x}Y_xO_{19}$ hexaferrite using Mössbauer spectroscopy, magnetometry, and X-ray diffraction showed that the isomorphic capacity of $BaFe_{12-x}Y_xO_{19}$ hexaferrite is low, and phase separation occurs in it starting from $x = 0.6$, with the formation of $Y_3Fe_5O_{12}$ and $BaFe_2O_4$ phases. The Mössbauer spectroscopy data show that in the studied range of substitutions, Y^{3+} ions enter the 12*k* position with the formation of an inequivalent position 12*k*' due to the breaking of magnetic bonds in the triad of 12*k* octahedra in Fe(12*k*)–O–Fe(12*k*) and the formation of Fe(12*k*)–O–Y(12*k*). Comparison of $BaFe_{12-x}Y_xO_{19}$ hexaferrite with $BaFe_{12-x}Al_xO_{19}$ and $BaFe_{12-x}Ga_xO_{19}$, which are magnetically hard and magnetically soft ferrite varieties, showed that yttrium-substituted hexaferrite can be classified as less magnetically hard than aluminum-substituted. Comparison of the results of studies of hexaferrites $BaFe_{12-x}Y_xO_{19}$ and $BaFe_{12-x}In_xO_{19}$ showed that, despite the identical radii of Y^{3+} and In^{3+} ions, their magnetic properties differ significantly, and

the main reason for this is the cation distribution and different electron configuration of Y^{3+} and In^{3+} ions.

FUNDING

The work was supported by the Russian Science Foundation (agreement no. 19-19-00694 of May 6, 2019).

CONFLICT OF INTERESTS

The authors declare that they have no conflicts of interests.

REFERENCES

1. R. C. Pullar, Prog. Mater. Sci. **57**, 1191 (2012).
2. Sh. Sh. Bashkirov, A. B. Liberman, and V. I. Sinyavskii, *Ferrite Magnetic Microstructure* (Kazan. Univ., Kazan', 1978) [in Russian].
3. V. V. Korovushkin, A. V. Trukhanov, V. G. Kostishin, I. M. Isaev, I. V. Shchetinin, N. M. Durov, A. Yu. Mironovich, I. O. Minkova, and K. A. Astapovich, Phys. Solid State **62**, 891 (2020).
4. V. V. Korovushkin, M. N. Shipko, V. G. Kostishin, I. M. Isaev, A. Yu. Mironovich, S. V. Trukhanov, and A. V. Trukhanov, Inorg. Mater. **55**, 1007 (2019).
5. V. V. Korovushkin, A. V. Trukhanov, M. N. Shipko, V. G. Kostishin, I. M. Isaev, A. Yu. Mironovich, and S. V. Trukhanov, Russ. J. Inorg. Chem. **64**, 574 (2019).
6. A. V. Trukhanov, S. V. Trukhanov, V. G. Kostishin, L. V. Panina, M. M. Salem, I. S. Kazakevich, V. A. Turchenko, V. V. Kochervinskii, and D. A. Krivchenya, Phys. Solid State **59**, 737 (2017).
7. A. V. Trukhanov, M. A. Darwish, L. V. Panina, A. T. Morchenko, V. G. Kostishyn, V. A. Turchenko, D. A. Vinnik, E. L. Trukhanova, K. A. Astapovich, A. L. Kozlovskiy, M. Zdorovets, and S. V. Trukhanov, J. Alloys Compd. **791**, 522 (2019).
8. M. A. Almessiere, Y. Slimani, H. Güngüne, A. Baykal, S. V. Trukhanov, and A. V. Trukhanov, Nanomaterias **9**, 24 (2019).
9. Y. Bakış, I. A. Auwal, B. Ünal, and A. Baykal, Composites, B **99**, 248 (2016).
10. S. Güner, I. A. Auwal, A. Baykal, and H. Sözeri, J. Magn. Magn. Mater. **416**, 261 (2016).
11. A. Auwal, H. Güngüneş, S. Güner, E. Sagar Shirsath, M. Sertkol, and A. Baykal, Mater. Res. Bull. **80**, 263 (2016).
12. R. Topkaya, I. Auwal, and A. Baykal, Ceram. Int. **42**, 16296 (2016).
13. K. M. Ur. Rehman, X. Liu, M. Li, S. Jiang, Y. Wu, C. Zhang, C. Liu, X. Meng, and H. Li, J. Magn. Magn. Mater. **426**, 183 (2017).
14. R. Alam, M. Tehrani, M. Moradi, E. Hosseinpour, and A. Sharbati, J. Magn. Magn. Mater. **323**, 1040 (2011).
15. F. Menil, J. Phys. Chem. Solids **46**, 763 (1985).
16. G. M. Bancroft, A. G. Maddok, and R. G. Burns, Geochim. Cosmochim. Acta **31**, 2219 (1967).
17. V. G. Kostishyn, V. V. Korovushkin, I. M. Isaev, and A. V. Trukhanov, East.-Eur. J. Enterp. Technol. **1**, 10 (2017).

Translated by G. Dedkov